PAPER

A hybrid upconversion nanoprobe for ratiometric detection of aliphatic biogenic amines in aqueous medium†

Shilpi Jaiswal, [ID] Subhankar Kundu, [ID] Sujoy Bandyopadhyay‡ and Abhijit Patra [ID] *

We fabricated an inorganic–organic hybrid upconversion nanoprobe for the ratiometric detection of aliphatic biogenic amines in water. The hybrid nanoprobe comprises a thiophene-based acceptor−π−donor−π-acceptor organic fluorescent dye, TDPM, and near-infrared light-absorbing upconversion nanoparticles (UCNPs). The organic dye was loaded into a mesoporous silica-coated UCNP (UCNP@mSiO$_2$) matrix to circumvent the issues of water insolubility and higher energy excitation. Yb^{3+} and Tm^{3+}-doped UCNPs exhibited dual emission bands at 475 and 645 nm upon excitation with a 980 nm laser. The significant spectral overlap between the absorption and the emission bands of TDPM and UCNPs, respectively, at 475 nm led to resonance energy transfer (RET) from the UCNPs to TDPM resulting in the quenching of the UCNP emission. In contrast, 'turn-on' emission was noticeable with the addition of aliphatic biogenic amines due to an inhibition of the RET. The emission at 645 nm remained unaffected during the energy transfer process making the hybrid probe a versatile platform for the ratiometric detection of different aliphatic biogenic amines. Furthermore, we explored the sensing of aliphatic biogenic amines in adulterated milk and rotten fish. The unique material attributes demonstrated in the current study hold promise for further development of real-time sensors and switches based on hybrid upconversion nanoprobes.

Introduction

Biogenic amines (BAs) are mostly generated due to the decarboxylation of amino acids through endogenous tissue metabolism or external microbial activity during food spoilage.[1,2] BAs regulate cell growth, and elevated levels of BAs may indicate bacterial infection and cancer.[3] On the other hand, aliphatic BAs, including spermine, cadaverine, and putrescine, are considered important biomarkers for monitoring food quality.[3,4] Thus, the selective and sensitive detection of aliphatic BAs is crucial and relevant both from academic and industrial perspectives.[5] Diverse methods like gas chromatography, high-performance liquid chromatography, electrolysis, and capillary electrophoresis have been employed to detect BAs.[5–7] However, the sophisticated instrumentation and long operational time are some of the major concerns. In this context, colorimetric and fluorometric sensing attract the attention of

the scientific community.[8–12] Even though colorimetric detection is cost-effective, it has a lower sensitivity. In contrast, fluorescence-based detection is highly sensitive. However, low water solubility, less Stokes shift, and high energy excitation commonly encountered in strongly fluorescent organic molecules induce a bottleneck.[13]

Recently, lanthanide-doped upconversion nanoparticles (UCNPs) have received considerable attention due to their unique features, such as low energy excitation (near-infrared), high energy emission (ultraviolet or visible), and high photochemical stability.[14–17] However, surface modification is essential to improve the water dispersibility and overcome the non-specificity of pristine UCNPs for the detection of analytes. Considering these facts, the concept of hybrid nanoprobes developed through the judicious integration of small functional organic molecules with UCNPs has emerged as a smart sensory platform for detecting different biomolecules and toxic elements.[18–22] The detection mechanism using hybrid upconversion nanoprobes mostly relies on the concept of energy transfer from UCNPs to organic fluorophores. In this context, the superiority of hybrid upconversion nanoprobes emerges from their large anti-Stokes shift emission, which rules out the possibility of co-excitation of both the donor (UCNPs) and acceptor (organic fluorophores) pairs, thus avoiding false-positive signals.[20] Li and co-workers demonstrated a Yb^{3+}-sensitized hybrid upconversion nanoprobe (UCNP@mSiO$_2$@-cyclodextrin@rhodamine B-derivative) for the ratiometric

Department of Chemistry, Indian Institute of Science Education and Research, Bhopal, Bhopal Bypass Road, Bhauri, Bhopal 462066, Madhya Pradesh, India. E-mail: abhijit@iiserb.ac.in

‡ Present address: Dr Sujoy Bandyopadhyay, Assistant Professor, Department of Chemistry, Indrashil University, Rajpur, Gujarat 382740, India.

sensing of nitric oxide.[21] Similarly, Zhang and co-workers reported a hybrid upconversion nanoprobe (UCNP@cyclodextrin@thiazole derivative) for the selective detection of Hg^{2+}.[22]

Herein, we fabricated a hybrid upconversion nanoprobe using mesoporous silica-coated UCNPs (UCNP@mSiO$_2$) and a thiophene-based acceptor–π-donor–π-acceptor (A–π-D–π-A) fluorescent organic dye, TDPM, for the detection of aliphatic BAs (Fig. 1). The surface modification of UCNPs through a mesoporous silica layer provided high physicochemical stability and water dispersibility and allowed further loading of fluorescent dyes. Consequently, the insolubility of TDPM in water and the higher energy excitation were circumvented by loading the dye into the UCNP@mSiO$_2$ matrix. The resultant hybrid upconversion nanoprobe (UCNP@mSiO$_2$@TDPM) was shown to exhibit ratiometric detection of aliphatic BAs in an aqueous medium. Furthermore, we employed the upconversion nanoprobe for the real-time detection of aliphatic BAs in adulterated milk and rotten fish. Different contaminants present in the test samples (fish, milk, and various food items) usually absorb in the UV-visible region. An advantage of the higher energy excitation of the developed probe is that the interference caused by such contaminants can be avoided.

Results and discussion

Design principle of the hybrid upconversion nanoprobe

The hybrid upconversion nanoprobe comprised UCNPs (NaYF$_4$, Yb^{3+}, and Tm^{3+}) and a mesoporous silica (mSiO$_2$) layer loaded
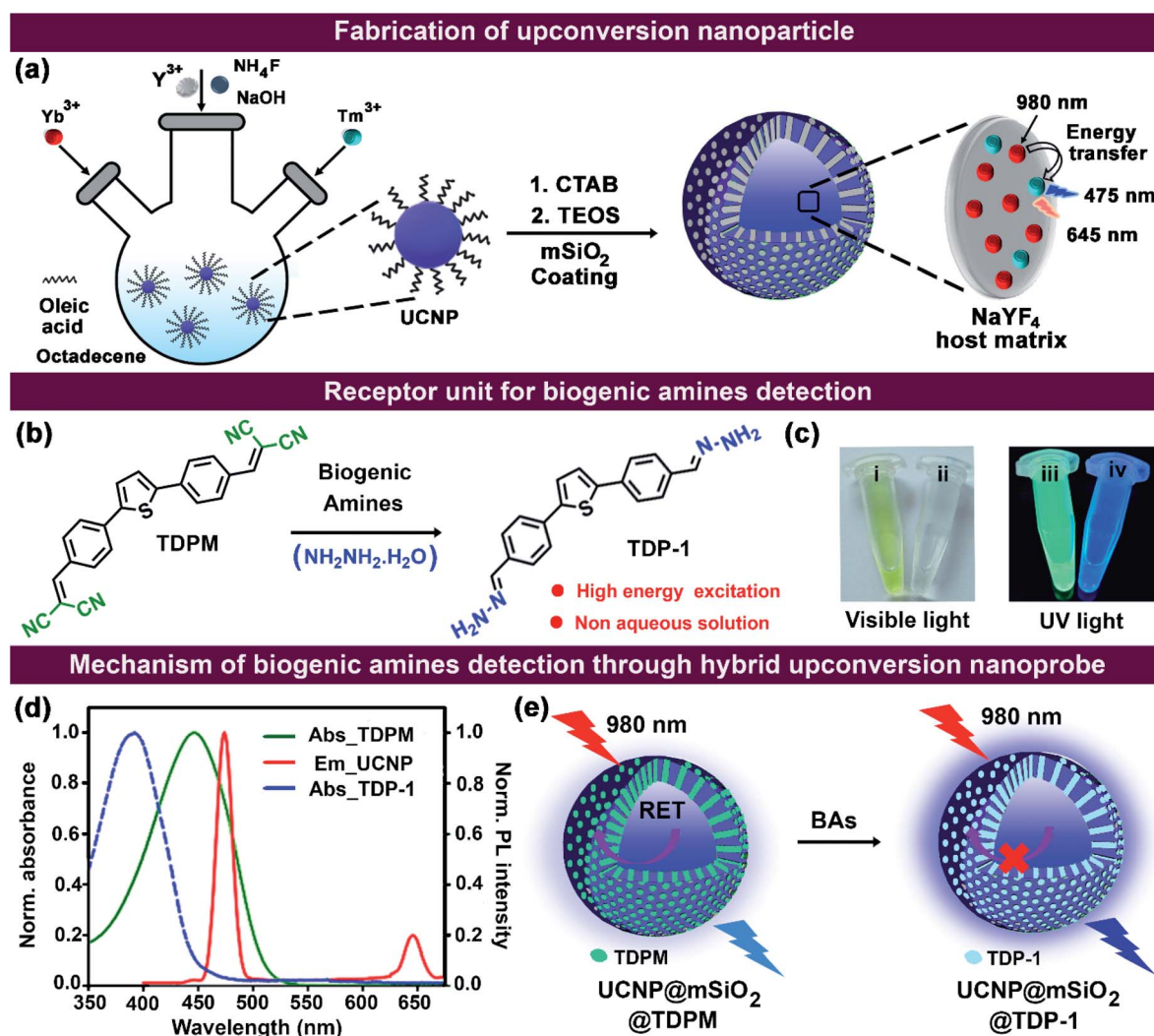

Fig. 1 (a) Schematic illustration depicting the fabrication routes of upconversion nanoparticles (UCNPs) and mesoporous silica-coated UCNPs (UCNP@mSiO$_2$). (b) Chemical transformation of a thiophene-based acceptor–π-donor–π-acceptor (A–π-D–π-A) fluorescent organic dye, TDPM, into TDP-1 upon the addition of biogenic amines; the representative chemical structure of TDP-1 is shown using hydrazine hydrate as an analyte. (c) The digital photographs of pristine TDPM solution (i and iii), and after the addition of aliphatic BAs (ii and iv) in DMSO under visible light (i and ii) and illumination at 365 nm (iii and iv). (d) Normalized UV-vis absorption spectrum of TDPM (5 μM, DMSO) in the absence (solid green line) and presence (blue dashed line) of aliphatic BAs (spermine). The solid red line represents the normalized upconversion luminescence (UCL) spectrum of the aqueous dispersion of UCNP@mSiO$_2$ (20 mg/3 mL). (e) Schematic representation illustrating the detection mechanism of biogenic amines (BAs) involving the organic–inorganic hybrid upconversion nanoprobe (UCNP@mSiO$_2$@TDPM) through the concept of resonance energy transfer (RET).
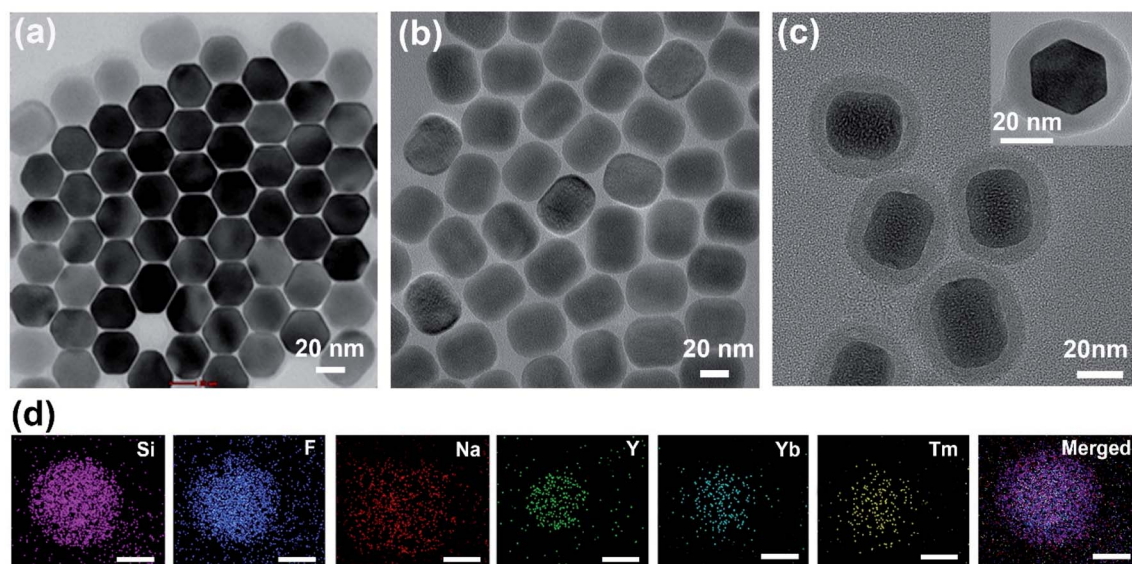
Fig. 2 Transmission electron microscopy (TEM) images of (a and b) UCNPs and (c) UCNP@mSiO$_2$; 10 μL of the respective samples (1 mg/3 mL, ethanol) were drop-cast on a carbon-coated Cu grid. (d) Energy dispersive X-ray (EDX) mapping of the elemental distribution of Si, F, Na, Y, Yb, and Tm in UCNP@mSiO$_2$ depicting the homogeneous distribution of constituent elements.

with an organic dye, TDPM (Fig. 1). NaYF$_4$, Yb^{3+}, and Tm^{3+} were employed as the host matrix, sensitizer, and activator, respectively. The excited-state energy transfer from Yb^{3+} to Tm^{3+} under the excitation of 980 nm led to the generation of two distinct emission bands at 475 and 645 nm due to the $^1G_4 \rightarrow {}^3H_6$ and $^1G_4 \rightarrow {}^3F_4$ transitions, respectively.[18,23] Furthermore, the silica coating on UCNPs reduced the surface quenching sites and enhanced the upconversion luminescence intensity.[15,24] The appreciable overlap between the UCNP@mSiO$_2$ emission band and the TDPM absorption band at 475 nm indicated the possibility of the resonance energy transfer (RET) process from the UCNPs to TDPM (Fig. 1d). A blue shift of the absorption band was noticeable upon the addition of the aliphatic BAs, including hydrazine (Fig. 1b–d). Hence, it was anticipated that the RET process would be inhibited upon the gradual addition of aliphatic BAs to the hybrid upconversion nanoprobe (Fig. 1d and e). Thus, the initial observations prompted us to fabricate the TDPM-loaded hybrid upconversion nanoprobe exhibiting promise for the 'turn-on' detection of aliphatic BAs in an aqueous medium under 980 nm excitation.

Synthesis and characterization of the nanoprobe

The oleic acid capped UCNPs were fabricated using the solvothermal method.[25] The morphology and size of UCNPs were characterized using transmission electron microscopy (TEM; Fig. 2a and b). The TEM images showed a mixed hexagonal and cubic morphology of UCNPs (Fig. 2a and b).[26] The average size of UCNPs was found to be 30 to 40 nm (the largest distance between two opposite faces) (Fig. 2a, b, and S1, ESI†). The lattice fringes in the high-resolution TEM images and the selected area electron diffraction (SAED) pattern confirmed the crystalline phase of UCNPs (Fig. S2, ESI†). Mesoporous silica was coated on the UCNP surface to improve the water dispersibility. It also

enhanced the upconversion luminescence intensity.[15,24] Fig. 2c depicts the TEM images of silica-coated UCNPs with an average size of 40–50 nm. The energy dispersive X-ray (EDX) mapping using TEM suggested the homogeneous distribution of different ions in UCNP@mSiO$_2$ (Fig. 2d).

The powder X-ray diffraction (PXRD) pattern revealed a highly crystalline and hexagonal phase of UCNPs (Fig. S3,† JCPDS no. 16-0334).[18,27] The broad new peak at 22° in the PXRD pattern for UCNP@mSiO$_2$ confirmed the coating of amorphous silica on the UCNP surface (Fig. 3a).[28] The thermal stability of both UCNPs and UCNP@mSiO$_2$ was up to 330 °C, as indicated by the thermogravimetric analysis (TGA) curves (Fig. S4, ESI†). The surface area and porosity of UCNP@mSiO$_2$ were estimated by using nitrogen adsorption and desorption isotherms at 77 K. The Brunauer–Emmett–Teller (BET) surface area of UCNP@mSiO$_2$ was found to be 74 m^2 g^{-1} with a total pore volume of 0.17 cm^3 g^{-1} at $P/P_0 = 0.95$. The hysteresis near $P/P_0 = 0.3$ and the steady increase in nitrogen adsorption even at higher relative pressure signified the mesoporous nature of the
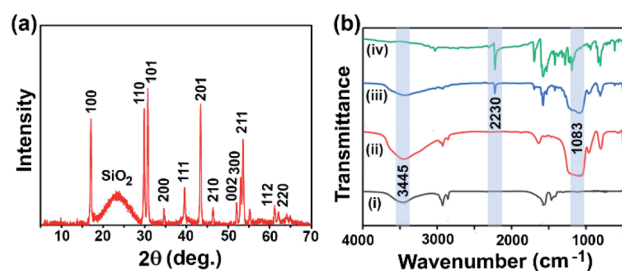

Fig. 3 (a) Powder X-ray diffraction (PXRD) pattern of UCNP@mSiO$_2$. (b) The comparative Fourier-transform infrared spectroscopy (FTIR) profiles of UCNPs (black, i), UCNP@mSiO$_2$ (red, ii), UCNP@mSiO$_2$@-TDPM (blue, iii), and TDPM (green, iv).

SiO_2 layer (Fig. S5a, ESI†). The pore size was calculated using the nitrogen sorption isotherm employing the nonlocal density functional theory (NLDFT) method. The major contribution of pore widths at 2.9 nm, along with the hierarchical distributions of mesopores, was observed (Fig. S5b, ESI†).

Afterward, TDPM was loaded into the mesoporous silica layer to fabricate a hybrid upconversion nanoprobe (UCNP@mSiO$_2$@TDPM). In a typical dye loading procedure, 20 mg of UCNP@mSiO$_2$ was dispersed into the solution of varying amounts of TDPM (0.05–0.35 mg in 3 mL DMSO). The resultant dispersions were sonicated for 1 h, followed by overnight stirring to obtain the hybrid nanoprobes. Furthermore, the hybrid upconversion nanoprobe (UCNP@mSiO$_2$@TDPM) was washed multiple times with DMSO and water to ensure the removal of unloaded dye (Fig. S7, ESI†). No significant change in the size and morphology was observed for TDPM encapsulated nanoparticles (Fig. S1c and S1d, ESI†). The encapsulation of TDPM into the UCNP@mSiO$_2$ matrix was monitored by Fourier-transform infrared (FTIR) spectroscopy. Fig. 3b shows the comparative FTIR profiles of UCNPs, UCNP@mSiO$_2$, UCNP@mSiO$_2$@TDPM, and TDPM. The broad peak at 3445 cm^{-1} was due to the stretching vibration of hydroxyl groups in oleic acid. The stretching vibrations of methylene groups in oleic acid were noticeable at 2924 and 2853 cm^{-1}.[28] The peak at 1565 cm^{-1} was attributed to the carbonyl functionality (C=O) of oleic acid.[28] The new peak at 1083 cm^{-1} was attributed to the stretching vibration of Si–O, which suggested the formation of a silica layer over UCNPs.[28,29] The peak at 2230 cm^{-1} was attributed to the –C≡N stretching vibration frequency of TDPM. Thus, the peaks at 2230 and 1083 cm^{-1} in UCNP@mSiO$_2$@TDPM confirmed the successful integration of TDPM and silica with UCNPs, respectively.

Optical properties of hybrid upconversion nanoprobes

TDPM-loaded hybrid upconversion nanoprobes were designated as HN1 to HN7, indicating the varied amount of encapsulated dye (HN1: 11 μg to HN7: 33 μg, per 20 mg of UCNP@mSiO$_2$). Repeated washing, along with centrifugation, followed by absorption measurements, confirmed the absence of any free dye in the aqueous dispersion of the hybrid nanoprobe (Fig. S7 and S8, ESI†). The TDPM loading amount was estimated through UV-Vis absorption spectroscopy (Fig. S9, ESI†). The increasing amount of TDPM loading into the UCNP@mSiO$_2$ matrix was reflected by the gradual rise in absorbance (Fig. 4a). The absorbance saturation for HN7 suggested a maximum dye loading capacity of 33 μg for UCNP@mSiO$_2$ (Fig. 4b). The spectral overlap between the UCNP emission and the TDPM absorption inferred the possibility of energy transfer from Tm^{3+} to TDPM dye, encapsulated in the porous SiO$_2$ matrix (Fig. 1d). Furthermore, to demonstrate the RET process, the upconversion luminescence was recorded for the aqueous dispersions of hybrid nanoprobes (HN1–HN7; Fig. 4c). The gradual decrease of UCNP emission (Tm^{3+}) at 475 nm and the increase of TDPM emission at 500–580 nm ascertained the RET process (Fig. 4c). Interestingly, the emission peak of Tm^{3+} at 645 nm remained unchanged, providing
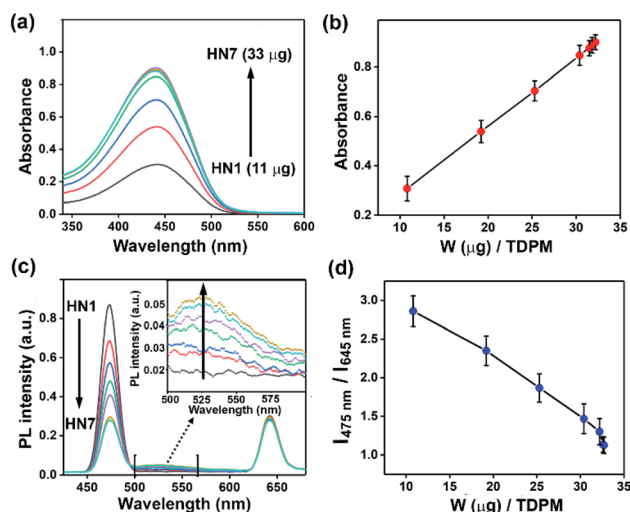

Fig. 4 (a) The absorption spectra of the hybrid upconversion nanoprobe in water (UCNP@mSiO$_2$: 20 mg/3 mL) with varying amounts of TDPM loading (HN1–HN7). (b) The linear relationship between the absorbance (λ_{max} = 445 nm) of the nanoprobe with varying TDPM loading amounts in the aqueous medium. The saturation in the absorbance depicting the maximum dye loading capacity for 20 mg of UCNP@mSiO$_2$. (c) The photoluminescence spectra (λ_{exc} = 980 nm) of the nanoprobes (HN1–HN7) with varying amounts of TDPM loading in the aqueous medium. Inset: zoomed-in view of the TDPM emission for the hybrid upconversion nanoprobe with varying amounts of dye loading. (d) The decrease in the ratio of the luminescence intensity ($I_{475\ nm}/I_{645\ nm}$) with increasing the loading amount of TDPM demonstrating the resonance energy transfer (RET) process. The bars represent the standard deviation of triplicate measurements.

scope to monitor the ratiometric change in fluorescence by tuning the energy transfer process (Fig. 4d).

Detection of aliphatic biogenic amines

The potential of the hybrid upconversion nanomaterial to detect aliphatic BAs in an aqueous medium was probed by monitoring the relative intensity of UCNP emission. The upconversion luminescence of UCNP@mSiO$_2$@TDPM (HN7) at 475 nm was recovered upon subsequent addition of spermine (aliphatic BA) due to the inhibition of RET (Fig. 5a). The mass spectrometric analysis revealed the chemical transformation of TDPM into the corresponding imine (analogous to TDP-1 obtained upon treatment with hydrazine,[30] Fig. 1b and Scheme S3, Fig. S10 and S11, ESI†) in the presence of spermine (Fig. S12 and S13, ESI†). The spectral mismatch between the absorption of the resultant imine and the UCNP emission was the reason behind the inhibition of the energy transfer leading to a 'turn on' upconversion luminescence response. The peak at 645 nm was used as a reference for the ratiometric detection ($I_{475\ nm}/I_{645\ nm}$) of aliphatic BAs (Fig. 5b). In contrast, TDPM alone was unsuitable for detecting aliphatic BAs in an aqueous medium due to its insolubility (Sec. 4.5, Fig. S14 and S15, ESI†). Furthermore, the RET process was probed through the decay analysis for UCNP (donor) emission at 475 nm using a time-correlated single-photon counting (TCSPC) set-up (Sec. 4.6, Fig. S16 and Scheme S4, ESI†). We observed a decrease in the
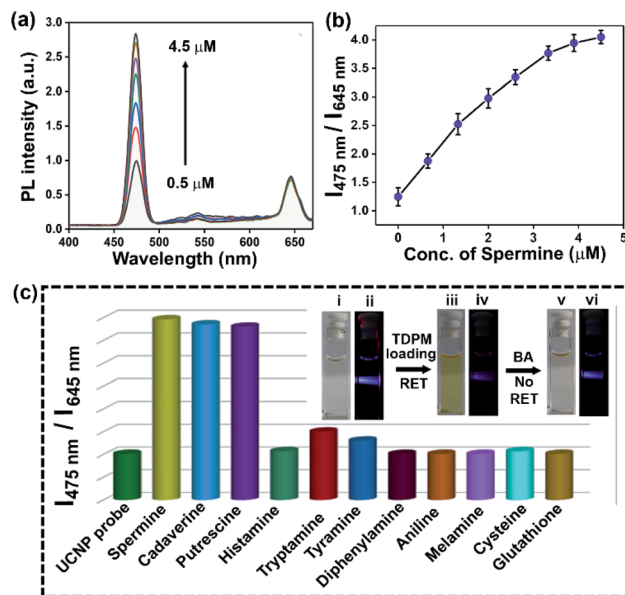
Fig. 5 (a) Upconversion luminescence spectra of the nanoprobe (20 mg/3 mL) with increasing concentration of spermine (aliphatic biogenic amine) in an aqueous medium. (b) The increase in the luminescence intensity ratio ($I_{475\ nm}/I_{645\ nm}$) with increasing concentration of spermine, demonstrating the inhibition of the RET process; the bars represent the standard deviation of triplicate measurements. (c) The ratiometric photoluminescence responses ($I_{475\ nm}/I_{645\ nm}$; $\lambda_{exc} = 980$ nm) of UCNP@mSiO$_2$@TDPM aqueous dispersion (20 mg/3 mL) upon the addition of diverse amines and amino acids (5 μM); inset: the digital photographs of UCNP@mSiO$_2$ (i and ii), UCNP@mSiO$_2$@TDPM (iii and iv), and aliphatic BA added UCNP@mSiO$_2$@TDPM (v and vi) aqueous dispersion under visible light (i, iii, and v) and illumination of a NIR laser (4 watt, $\lambda_{exc} = 980$ nm; ii, iv, and vi); the intensity variation in upconversion luminescence demonstrating the RET.

lifetime of Tm^{3+} (donor, $\lambda_{em} = 475$ nm) from 250 to 169 μs in the hybrid upconversion nanoprobe upon the gradual increase of the TDPM loading (HN1 to HN7) compared to that of the pristine mesoporous silica-coated UCNPs (Fig. S16, ESI†). The results unambiguously ascertained the energy transfer from UCNPs to TDPM. Moreover, the concomitant increase in the decay time for Tm^{3+} emission was observed upon gradual addition of a biogenic amine (spermine, 0.5–4.5 μM) to the dispersion of the hybrid nanoprobe (HN7), indicating an inhibition of the energy transfer process.

The selectivity of aliphatic BA detection was assessed by comparing the upconversion luminescence response of UCNP@mSiO$_2$@TDPM in the presence of a diverse range of analytes, including aliphatic biogenic amines, aromatic biogenic amines, and metal ions (Fig. S17–S19, ESI†). A significant enhancement of the ratiometric upconversion luminescence signal was noticeable upon the addition of aliphatic BAs (Fig. 5c). Both the electronic and the steric factors of amines governed the sensitivity of the hybrid upconversion nanoprobes. The higher nucleophilicity and less steric hindrance of aliphatic BAs and biogenic polyamines like spermine than that of their aromatic counterpart might be the reason behind the observed sensing behaviour (Table S1, ESI†).[31] The limit of

detection (LOD) for spermine was found to be 0.11 ± 0.02 μM (Fig. S20, ESI†). Additionally, the LOD was calculated for other aliphatic biogenic amines like cadaverine and putrescine (Fig. S21 and S22, ESI†).

Detection of spermine in milk and fish

We employed the upconversion nanoprobe for the sensing of spermine in spiked milk to evaluate the practical applicability of the developed hybrid nanomaterial. Fresh milk was treated with trichloroacetic acid following earlier reports.[32] The upconversion luminescence intensity was monitored before and after adding the pre-treated milk sample (50 μL) into the aqueous dispersion of UCNP@mSiO$_2$@TDPM (100 mg/3 mL). The negligible change in the luminescence signal indicated the absence of aliphatic BAs in the treated milk samples (Fig. 6a and S23, ESI†). Furthermore, the milk sample was spiked with varying concentrations of spermine. A progressive enhancement in the upconversion luminescence intensity was observed upon the addition of the spiked milk samples (Fig. 6a). The amount of spermine in the spiked milk samples was estimated to be within the range of 100 to 104%, with the relative standard deviation (RSD) values in the range of 1.4 to 3.5% (Fig. 6b and Table S2, ESI†). The detection limit of spermine (0.11 μM) and cadaverine (0.13 μM) using the hybrid upconversion nanoparticles suggests that the probe can detect the minimum concentration of cadaverine (0.13 mg kg^{-1}, 1.2 μM) and spermine (0.86 mg kg^{-1}, 4.2 μM) found in fresh milk.[33] Hence, the UCNP@SiO$_2$@TDPM probe can be used as a ratiometric sensor for monitoring the freshness of milk samples (Sec. 5, ESI†).

In addition, the hybrid upconversion nanoprobe was employed for monitoring the freshness of raw fish. Rotten fish contains an elevated level of BAs.[34] The fish sample and pellet made up of UCNP@mSiO$_2$@TDPM were stored in Petri dishes separately at room temperature (RT $\sim$ 25 °C) and −20 °C for 0 to 4 days (Fig. 7). The excess BAs in rotten fish after storage for 4 days led to the chemical transformation of TDPM. An increase in the upconversion luminescence was observed under the illumination of 980 nm for the pellet kept at room temperature. It was due to the formation of biogenic amines from the rotten fish in 4 days resulting in the inhibition of the RET process (Panel A, Fig. 7a–c). In contrast, no significant visual change in upconversion luminescence was noticeable for the pellet with
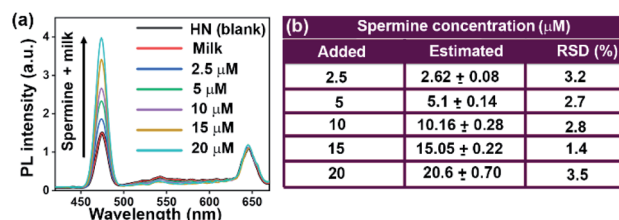

Fig. 6 (a) The upconversion luminescence spectra of pristine UCNP@mSiO$_2$@TDPM in water (HN, 100 mg/3 mL) and with varying amounts of spiked milk (spermine: 2.5–20 μM). (b) Tabular representation of the relative standard deviation (RSD) of the estimated biogenic amine (spermine) in pre-treated milk employing the hybrid upconversion nanoprobe.
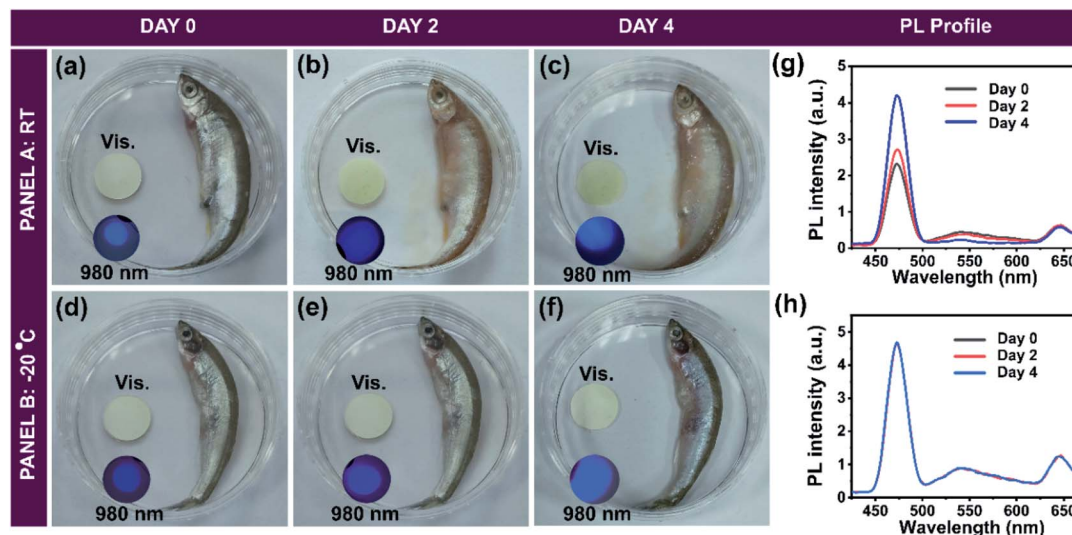
Fig. 7 Monitoring of fish freshness under different storage conditions at room temperature (RT) and −20 °C using the hybrid upconversion nanoprobe pellet (40 mg). (a–f) The digital photographs of the nanoprobe pellets with a variation of the storage time from 0 to 4 days demonstrating gradually increasing (Panel A; RT; a–c) and invariant (Panel B, −20 °C; d–f) upconversion luminescence under illumination at 980 nm with a NIR laser beam (4 watt). (g) The enhancement in the luminescence intensity (Panel A; RT) with the variation of the storage time from 0 to 4 days, indicating the inhibition of the RET process due to the higher concentration of BAs in rotten fish. (h) In contrast, the unchanged PL intensity signal (Panel B), depicting a facile RET process even after 4 days due to the freshness of the stored fish at −20 °C.

fish stored at −20 °C after 4 days (Panel B, Fig. 7d–f). The results were also corroborated through upconversion luminescence intensity *vs.* wavelength plots (Fig. 7g and h). Thus, UCNP@mSiO$_2$@TDPM can be used as a marker for monitoring the freshness of fish and food beverages (Tables S3 and S4, ESI†).

Conclusion

In summary, an inorganic–organic hybrid upconversion nanoprobe (UCNP@mSiO$_2$@TDPM) was fabricated for the ratiometric detection of aliphatic biogenic amines in aqueous medium. The probe consisted of mesoporous silica-coated upconversion nanoparticles [UCNP(NaYF$_4$, Yb^{3+}, Tm^{3+})@mSiO$_2$] and a thiophene containing π-conjugated organic molecule, TDPM. A chemical transformation of TDPM into the corresponding imine form was noticeable upon the addition of aliphatic biogenic amines. The significant overlap between the UCNP@mSiO$_2$ emission and TDPM absorption was used to demonstrate the resonance energy transfer process. A decrease in the upconversion emission intensity at 475 nm was noticeable upon increasing the concentration of TDPM loaded into UCNP@mSiO$_2$. In contrast, the energy transfer ceased in the presence of aliphatic biogenic amines. Consequently, a gradual increase of the 475 nm emission band along with an unaltered 645 nm band of the hybrid upconversion nanoprobe offered a viable platform for the ratiometric detection of aliphatic biogenic amines in an aqueous medium. Moreover, we demonstrated the detection of aliphatic biogenic amines in adulterated milk and rotten fish, signifying the potential for further development of diverse hybrid upconversion nanoprobes as real-time sensors and switches.

Experimental section

Fabrication of upconversion nanoparticles (UCNPs)

The fabrication of upconversion nanoparticles was carried out following a reported procedure.[25] 0.78 mmol of YCl$_3$·6H$_2$O, 0.20 mmol of YbCl$_3$·6H$_2$O, and 0.02 mmol of TmCl$_3$ were dissolved in a minimum volume of water to make a homogeneous solution. The solution was taken into a three-neck round-bottom (RB) flask and was heated up to 120 °C. Subsequently, 6 mL of oleic acid and 15 mL of 1-octadecene were added to the RB flask and the solution was heated to 160 °C for 2 h. Afterward, the reaction mixture was brought to room temperature. Then, a methanol solution of 4 mmol of ammonium fluoride and 2.5 mmol of sodium hydroxide was added to the reaction mixture, followed by 30 min stirring. The mixture was heated up to 110 °C. Furthermore, the solution was degassed and kept under a nitrogen atmosphere for 10 min. Finally, the temperature was slowly increased to 280 °C, and heating was continued for 120 min. Then the reaction mixture was cooled to room temperature. The as-prepared UCNPs (NaYF$_4$, Yb^{3+}, and Tm^{3+}) were collected by centrifugation at 6000 rpm for 15 min and washed multiple times with hexane and ethanol.

Fabrication of silica-coated UCNPs (UCNP@mSiO$_2$)

10 mg of UCNPs were dispersed in 2 mL of cyclohexane. Then, the dispersion was added into an aqueous solution of CTAB (0.1 g in 20 mL of water) and was vigorously stirred at room temperature to evaporate cyclohexane. Furthermore, a solution containing water (20 mL), ethanol (3 mL), and NH$_4$OH (150 μL, 30%) was added to the above reaction mixture. Then, 150 μL tetraethyl orthosilicate (TEOS) was added dropwise, and the

resultant mixture was stirred for 48 h. The product was centrifuged at 6000 rpm for 10 min and washed multiple times with ethanol.[25]

Loading of TDPM into the UCNP@mSiO$_2$ matrix

The loading of TDPM into the UCNP@mSiO$_2$ matrix was carried out by a simple stirring and centrifugation method. In a typical dye loading procedure, 20 mg of silica-coated UCNPs was taken into seven different RB flasks. Then, different amounts of TDPM (0.05, 0.1, 0.15, 0.20, 0.25, 0.30, and 0.35 mg in 3 mL DMSO) were added into the respective RB flasks. The mixture was sonicated for 1 h and kept stirring overnight. Finally, the different suspensions were centrifuged at 6000 rpm for 10 min and washed multiple times with DMSO and water.

Milk sample treatment

2 mL of 20% trichloroacetic acid was added to 10 mL of milk sample for protein coagulation.[32] Afterward, the milk sample was centrifuged at 10 000 rpm for 30 min. The supernatant was then filtered through a 0.22 μm membrane to remove all the interfering substances in the milk. Furthermore, the milk sample was spiked with varying concentrations of spermine from 2.5 μM to 20 μM.

Conflicts of interest

There is no conflict to declare.

Acknowledgements

References

1 (a) A. R. Shalaby, Food Res. Int., 1996, 29, 675; (b) A. Naila, S. Flint, G. Fletcher, P. Bremer and G. Meerdink, J. Food Sci., 2010, 75, 139.

2 (a) H. Zhong, C. Liu, W. Ge, R. Sun, F. Huang and X. Wang, ACS Appl. Mater. Interfaces, 2017, 9, 22875; (b) R. Jia, W. Tian, H. Bai, J. Zhang, S. Wang and J. Zhang, Nat. Commun., 2019, 10, 795.

3 (a) B. Bao, L. Yuwen, X. Zheng, L. Weng, X. Zhu, X. Zhan and L. Wang, J. Mater. Chem., 2010, 20, 9628; (b) R. R. Kothur, B. A. Patel and P. J. Cragg, Chem. Commun., 2017, 53, 9078.

4 (a) M. H. SillaSantos, Int. J. Food Microbiol., 1996, 29, 213; (b) Y. Özogul and F. Özogul, in Biogenic Amines in Food: Analysis, Occurrence and Toxicity, The Royal Society of Chemistry, 2020.

5 A. Önal, Food Chem., 2007, 103, 1475.

6 R. Draisci, G. Volpe, L. Lucentini, A. Cecilia, R. Federico and G. Palleschi, Food Chem., 1998, 62, 225.

7 T. Esatbeyoglu, A. Ehmer, D. Chaize and G. Rimbach, J. Agric. Food Chem., 2016, 64, 2105.

8 A. P. Silva, H. Q. N. Gunaratne, T. Gunnlaugsson, A. J. M. Huxley, C. P. McCoy, J. T. Rademacher and T. E. Rice, Chem. Rev., 1997, 97, 1515.

9 (a) H. N. Kim, Z. Guo, W. Zhu, J. Yoon and H. Tian, Chem. Soc. Rev., 2011, 40, 79; (b) X. Zhang, J. Yin and J. Yoon, Chem. Rev., 2014, 114, 4918; (c) D. Wu, A. C. Sedgwick, T. Gunnlaugsson, E. U. Akkaya, J. Yoon and T. D. James, Chem. Soc. Rev., 2017, 46, 7105.

10 (a) M. H. Lee, J. S. Kim and J. L. Sessler, Chem. Soc. Rev., 2015, 44, 4185; (b) S. Singh, D. Kim, H. Seo, S. W. Choa and K. H. Ahn, Chem. Soc. Rev., 2015, 44, 4367; (c) J. Oh, H. Rhee and J. Hong, in Synthetic Receptors for Biomolecules: Design Principles and Applications, The Royal Society of Chemistry, 2015; (d) J. Zhou and H. Ma, Chem. Sci., 2016, 7, 6309; (e) B. Liu, J. Zhuang and G. Wei, Environ. Sci.: Nano, 2020, 7, 2195.

11 (a) A. Deshmukh, S. Bandyopadhyay, A. James and A. Patra, J. Mater. Chem. C, 2016, 4, 4427; (b) P. Pallavi, V. Kumar, M. W. Hussain and A. Patra, ACS Appl. Mater. Interfaces, 2018, 10, 44696; (c) A. Weißenstein, C. R. Saha-Möller and F. Würthner, Chem.–Eur. J., 2018, 24, 8009.

12 (a) V. Kumar, B. Sk, S. Kundu and A. Patra, J. Mater. Chem. C, 2018, 6, 12086; (b) V. Kumar, S. Kundu, B. Sk and A. Patra, New J. Chem., 2019, 43, 18582; (c) C. Guo, A. C. Sedgwick, T. Hirao and J. L. Sessler, Coord. Chem. Rev., 2021, 427, 213560.

13 J. Zhou, Q. Liu, W. Feng, Y. Sun and F. Li, Chem. Rev., 2015, 115, 395.

14 F. Auzel, Chem. Rev., 2004, 104, 139.

15 G. Chen, H. Qiu, P. N. Prasad and X. Chen, Chem. Rev., 2014, 114, 5161.

16 (a) W. Zheng, P. Huang, D. Tu, E. Ma, H. Zhu and X. Chen, Chem. Soc. Rev., 2015, 44, 1379; (b) M. H. Chan and R. S. Liu, Nanoscale, 2017, 9, 18153; (c) M. Safdar, A. Ghazy, M. Lastusaari and M. Karppinen, J. Mater. Chem. C, 2020, 8, 6946.

17 (a) B. Gu and Q. Zhang, Adv. Sci., 2018, 5, 1700609; (b) S. Wen, J. Zhou, K. Zheng, A. Bednarkiewicz, X. Liu and D. Jin, Nat. Commun., 2018, 9, 2415; (c) G. Tessitore, G. A. Mandl, M. G. Brik, W. Park and J. A. Capobianco, Nanoscale, 2019, 11, 12015; (d) Y. Wong, S. Pang, M. Tsang, Y. Liu, H. Huang, S. Yu and J. Hao, Nanoscale Adv., 2019, 1, 265.

18 Z. Li, T. Liang, S. Lv, Q. Zhuang and Z. Liu, J. Am. Chem. Soc., 2015, 137, 11179.

19 (a) S. Wu, X. J. Kong, Y. Cen, J. Yuan, R. Q. Yu and X. Chu, Nanoscale, 2016, 8, 8939; (b) O. Dukhno, F. Przybilla, M. Collot, A. Klymchenko, V. Pivovarenko, M. Buchner, V. Muhr, T. Hirsch and Y. Mély, Nanoscale, 2017, 9, 11994; (c) Y. Liu, Q. Ouyang, H. Li, Z. Zhang and Q. Chen, ACS Appl. Mater. Interfaces, 2017, 9, 18314; (d) M. K. Mahata and K. T. Lee, Nanoscale Adv., 2019, 1, 2372.

20 E. Jo, J. Byun, H. Mun, D. Bang, J. H. Son, J. Y. Lee, L. P. Lee and M. Kim, *Anal. Chem.*, 2018, **90**, 716.

21 N. Wang, X. Yu, K. Zhang, C. A. Mirkin and J. Li, *J. Am. Chem. Soc.*, 2017, **139**, 12354.

22 B. Gu, Y. Zhou, X. Zhang, X. Liu, Y. Zhang, R. Marks, H. Zhang, X. Liu and Q. Zhang, *Nanoscale*, 2016, **8**, 276.

23 J. Peng, W. Xu, C. L. Teoh, S. Han, B. Kim, A. Samanta, J. C. Er, L. Wang, L. Yuan, X. Liu and Y. Chang, *J. Am. Chem. Soc.*, 2015, **137**, 2336.

24 (*a*) A. Kar and A. Patra, *Nanoscale*, 2012, **4**, 3608; (*b*) S. Liu, L. Zhang, T. Yang, H. Yang, K. Y. Zhang, X. Zhao, W. Lv, Q. Yu, X. Zhang, Q. Zhao, X. Liu and W. Huang, *ACS Appl. Mater. Interfaces*, 2014, **6**, 11013; (*c*) A. Kar, S. Kundu and A. Patra, *ChemPhysChem*, 2015, **16**, 505; (*d*) B. Kumar, V. S. S. Rathnam, S. Kundu, N. Saxena, I. Banerjee and S. Giri, *ChemNanoMat*, 2018, **4**, 583.

25 M. K. Gnanasammandhan, N. M Idris, A. Bansal, K. Huang and Y. Zhang, *Nat. Protoc.*, 2016, **4**, 688.

26 (*a*) H. Mai, Y. Zhang, R. Si, Z. Yan, L. Sun, L. You and C. Yan, *J. Am. Chem. Soc.*, 2006, **128**, 6426; (*b*) R. Arppe, T. Näreoja, S. Nylund, L. Mattsson, S. Koho, J. M. Rosenholm, T. Soukka and M. Schäferling, *Nanoscale*, 2014, **6**, 6837.

27 T. Ma, Y. Ma, S. Liu, L. Zhang, T. Yang, H. Yang, W. Lv, Q. Yu, W. Xu, Q. Zhao and W. Huang, *J. Mater. Chem. C*, 2015, **3**, 6616.

28 R. Han, J. Shi, Z. Liu, Y. Hou and Y. Wang, *ACS Biomater. Sci. Eng.*, 2018, **4**, 3478.

29 (*a*) M. Wang, C. Mia, Y. Zhang, J. Liu, F. Lia, C. Mao and S. Xu, *J. Phys. Chem. C*, 2009, **113**, 19021; (*b*) A. Sedlmeier and H. H. Gorris, *Chem. Soc. Rev.*, 2015, **44**, 1526.

30 (*a*) M. Sun, J. Guo, Q. Yang, N. Xiao and Y. Li, *J. Mater. Chem. B*, 2014, **2**, 1846; (*b*) X. Yang, Y. Liu, Y. Wu, X. Ren, D. Zhang and Y. Ye, *Sens. Actuators, B*, 2017, **253**, 488.

31 S. Jindal, V. K. Maka and J. N. Moorthy, *J. Mater. Chem. C*, 2020, **8**, 11449.

32 P. Leng, F. Zhao, B. Yin and B. Ye, *Chem. Commun.*, 2015, **51**, 8712.

33 D. M. Linares, M. C. Martin, V. Ladero, M. A. Alvarez and M. Fernandez, *Food Sci. Nutr.*, 2011, **51**, 691.

34 J. Donthuan, S. Yunchalard and S. Srijaranai, *Anal. Methods*, 2014, **6**, 1128.